Figure 3.1: LEP vacuum chamber cross section (courtesy of CERN).

values. Completely covering the inner surface of a chamber with St 707 strips activated at 400°C, it was possible to reach pumping speed values larger than 10000 $\ell \cdot s^{-1}$ per linear meter, resulting in pressure values lower than 10^{-13} $Torr$. In order to increase the pumping speeds and to reduce the dimensions of the pump the distance between the pump and the wall of the chamber was progressively reduced. The limitation to this approach was that, while the pumping efficiency was improved, the gas load in the system was not reduced. The solution to this problem came with the introduction of the idea to deposit a NEG thin film directly on the wall of the chamber, significantly reducing the outgassing rate of the system. This technology was developed in conjunction with the design and development of LHC, in which is nowdays still employed to provide UHV in the room temperature sections.

3.3 Selection of getter materials

Activation temperature The activation temperature T_a of the NEG material has to be compatible with the maximum baking temperature of the vacuum chambers. Thus temperatures lower than 400°C are required. Thanks to the evolution of NEG materials, T_a has been lowered to 200°C, allowing the employment of materials like aluminium or copper as substrate of the coating.

Solubility limit The activation mechanism consists in the dissolution of the surface passivation oxide layer into the material bulk. In order to make it possible the selected material has to have a reasonable solubility limit to allow the dissolution process. Every time that NEG material is exposed to air (a procedure called venting) a new oxide layer is formed on the surface, so, in order to accommodate the oxygen accumulation due to many venting cycles, a higher solubility limit is needed. Considering that the oxide layer formed during air exposure is 2-3 nm thick, after ten venting cycles the oxygen concentration in a 1 micron-thick film would be the 2-3%. To guarantee a longer NEG lifetime a 10% solubility limit is desirable.

In order to pump the main gas present in a UHV system, namely CO, CO_2 and H_2, the NEG material should have a high reactivity, so large enthalpies of adsorption are required. Furthermore, to provide a low H_2 partial pressure in the system, H_2 dissociation pressure has to be low.

Other selection criteria Other properties related to the deposition process and on the kind of application of the NEG coating have to be considered. Some features such as a good adhesion to the substrate, high melting point and high mechanical resistance are thus needed. In the specific case of particle accelerators NEG material should be non-magnetic, non-toxic, non-pyrophoric and present low photoelectric and secondary electron emission yield.

To fulfil all the requirements listed above, many different materials and alloys were tested. Among them combinations of metals of the 4th and 5th group of the periodic table were selected for their properties. In fact transi-

tion metals of the 4th group (Ti, Zr, Hf) present a solubility limit exceeding 10%, while those of the 5th group (V, Nb, Ta) provide much higher oxygen diffusivity but a lower oxygen solubility limit. A summary of the activation temperatures of different alloys is shown in Figure 3.2.

Getter	$T_{ACTIVATION}$ [°C] for 24 h heating
St101 $Zr_{84}Al_{16}$ (weight content)	600
St707 $Zr_{70}V_{24.6}Fe_{5.4}$ (weight content)	350
TiZr (atomic content)	250
$Ti_{30}Zr_{30}V_{40}$ (atomic content)	180

Figure 3.2: Summary of the activation temperature T_a of some NEG materials.

3.4   *TiZrV* films

Among all the alloys tested to fulfil the requirements for the application in the LHC machine, a ternary alloy of titanium, zirconium and vanadium was found to display full activation after 4 h heating at 200 °C, fulfilling all the requirements listed in Section 3.3. Thus deeper studies were performed on this alloy to better understand its properties and possibly further improve it.

Deposition method

The deposition of $TiZrV$ thin film on the inner wall of the camber is made by magnetron sputtering. Magnetron sputtering is a plasma coating process whereby sputtering material is ejected due to bombardment of ions to the target surface. The vacuum chamber is filled with an inert gas, such as argon. By applying a high voltage, a glow discharge is created, resulting in acceleration of ions to the target surface and a plasma coating. The argon-ions will eject sputtering materials from the target surface (sputtering), resulting in a sputtered coating layer on the target. A magnetic field is applied in order to keep the plasma in front of the target, intensifying the bombardment of ions. The cathode consists of three twisted wires of Ti, Zr and V respectively. The composition of the deposed alloy can be changed changing the diameter or the number of wires.

Activation temperature

The activation temperature can be affected changing the composition of the alloy. A lot of different compositions were tested in order to find the lowest activation temperature. From these studies it was found out that there are many possible compositions having the same activation temperature, most of them resulting in a low percentage of Ti in the alloy. X-ray analysis indicates that the low activation temperature is linked to amorphous or nano-crystal structure, which particularly enhances oxygen diffusion along grain boundaries [6]. In the case of an alloy with $Ti_{30\%}Zr_{20\%}V_{50\%}$ it was seen that the material is fully activated at 180 °C (Figure 3.3).

The characterization of samples of different composition were done using Auger Electron Spectroscopy (AES). Heating favours the increase of the metallic Zr peak with respect to the Zr oxide peak. Different samples have reached the same level of activation when their relative increase of this peak is the same. The ratio R between the intensity of these two peaks gives an indication of the activation level into the sample. Depending on the value of R the samples can be divided in two classes: low activation temperature ($R > 0.5$) and high activation temperature ($R < 0.5$)(Figure 3.4).
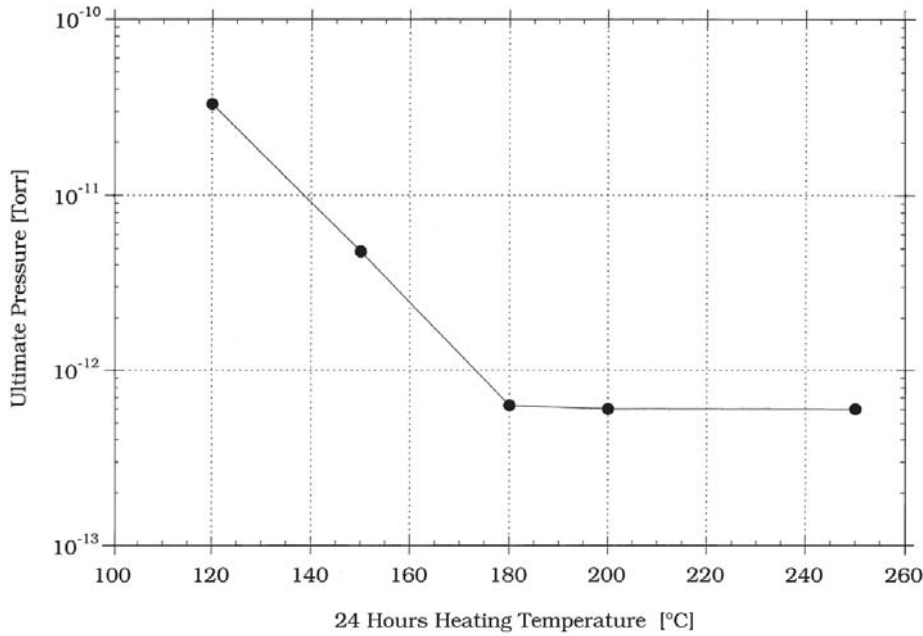
Figure 3.3: Ultimate pressures measured in NEG coated chamber of 54 mm diameter after 24 h activation as function of the heating temperature [6].

Surbstrate

Surface roughness plays an important role in the definition of the molecular sticking factors. Multiple reflections may take place when a molecule hits a rough surface, and its capture probability is enhanced correspondingly. The roughness of a coating depends on many parameters. Among them the characteristics of the substrate have to be taken into account. It has been observed that materials such as beryllium and aluminium favour the formation of a "cauliflower" structure with an appreciable roughness [6]. Stainless steel and copper on the other side tend to generate a smooth coating. Another important parameter is the temperature of the substrate during the coating process. The variation of the temperature strongly modify the film morphology. The enhanced mobility due to high temperature favours coalescence which results in rough structures [22]. The roughness of the surface increases the roughness of the film, then resulting in better pumping properties.

It is possible to observe in Figure 3.5 that the roughness of the film drastically increase for temperature higher than 200°C.
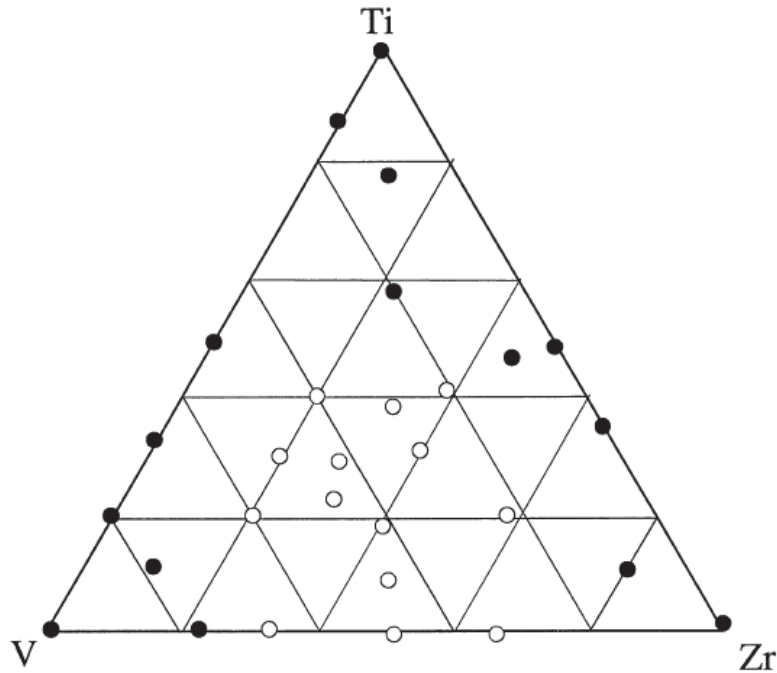
Figure 3.4: Quality-composition map of TiZrV thin films produced by means of the three-cathode sputtering system. The white dots represent samples with $R > 0.5$ while the black ones $R < 0.5$ [6].

Discharge gas

Because of their high mass, noble gases are used to generate the plasma during the coating process. When the discharge ions impinge the cathode they can be bounced back with enough kinetic energy to be implanted in the target surface. During operations the desorption of these discharge noble gases, which are not pumped by NEG, can compromise the maintenance of the required pressure value in the vacuum system.

It was observed that the employment of heavy noble gases reduces the amount of discharge gas into the film. It has been proved that in case of TiZrV coating produced by magnetron sputtering an Ar content of about 3500 ppm has been measured, meanwhile the content of Kr is two orders of magnitude lower. Thus Kr was chosen for the the coating process [24].
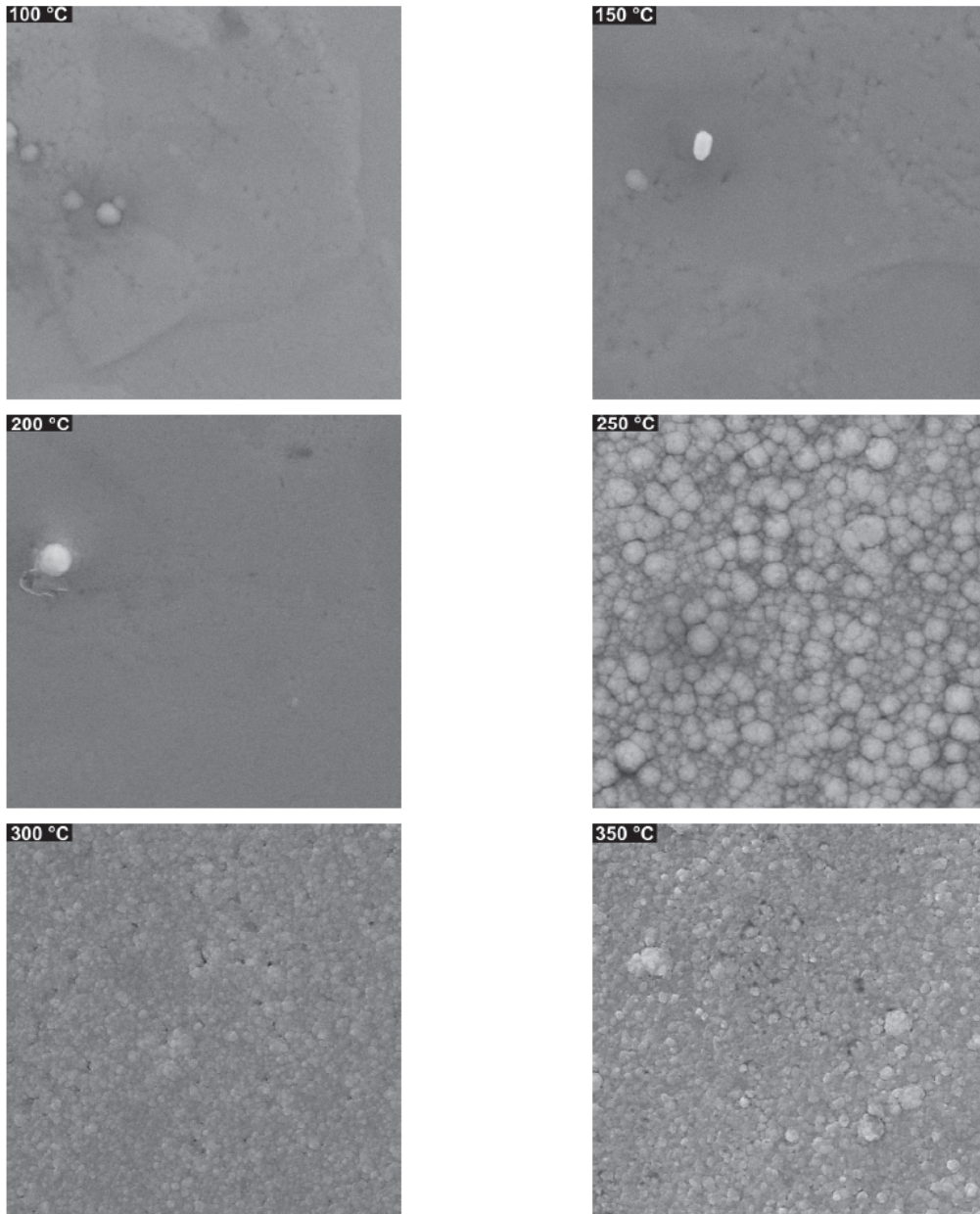
Figure 3.5: $TiZrV$ thin film sputtered on smooth copper substrate at substrate temperatures ranging form 100 to 350°C.

Chapter 4

Long Shutdown 1

During operations of the LHC in September 2008 a weld in a superconducting wire connecting two magnets heated above its operating temperature. That in effect turned the wire into a resistor, causing a massive 8.7 kA of power to arc through the liquid helium and puncture into the surrounding vacuum vessel. This accident lead to a one year stop of the LHC in order to repair the damaged components and consolidate the magnets interconnections.

Figure 4.1:   Visible damage to the LHC magnets in sector 3-4 of the LHC on November 12th, 2008. On September 19th, 2008, as the LHC was being switched on, a faulty electrical connection between two of the accelerator's magnets caused a large helium leak, which violently vented 6 tons of helium into the tunnel. The resulting temperature rise damaged some 53 magnets (courtesy of CERN).

After this accident it was decided to plan a 20 month stop in 2013, Long Shutdown 1. The LS1 was triggered by the need to consolidate the magnet interconnections to allow the LHC to operate at the design energy of 14 TeV in the centre-of-mass. It became rapidly a major shutdown, which, in addition, includes other repairs, consolidations, upgrades and cabling across the whole accelerator complex and the associated experimental facilities. LS1 has seen a massive programme of maintenance for the LHC and its injectors [12]. The main intervention brought out during the LS1 are summarized in Figure 4.2.

Figure 4.2: Percentage of opened sectors during LS1.

4.1 Interventions in the LSS

Despite the good performance of the beam vacuum system during Run 1, some consolidation, repair and upgrade are required in the LSS. During LS1 148 room temperature vacuum sectors were opened and recommissioned to allow both vacuum related repair and activities on other systems [29]. Figure 4.3 shows a summary of the percentage of open sectors during LS1. About

80% of the sectors, corresponding to 5.1 km in length, were opened during this period.
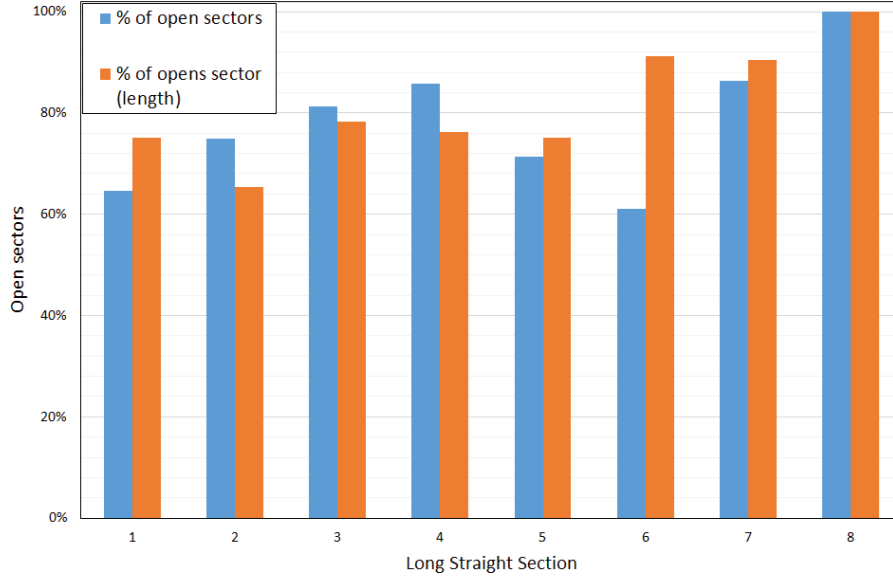
Figure 4.3: Percentage of opened sectors during LS1.

The 85% of the room temperature sectors is coated with a 1 μm TiZrV film, which provides most of the pumping speed. The sectors were vented to N_2 in order to allow the interventions, thus saturating the NEG coating and making necessary a new bake-out and activation cycle. Figure 4.4 and 4.5 show the number of venting, bake-out and activation cycles undergone by the room temperature sectors before LS1.

It is possible to notice that more than the 70% of the sectors were vented, baked and activated more than once since LHC construction.

Considering that two more Long Shutdowns, which will imply interventions and thus more venting and activation cycles all around the machine, are planned for the LHC in the next years (LS2 in 2018 and LS3 in 2025), it becomes of primary importance to foresee how the vacuum properties will evolve, in order to properly plan the eventual substitution of NEG coated chambers. From this considerations comes the needing to carry out the present study.
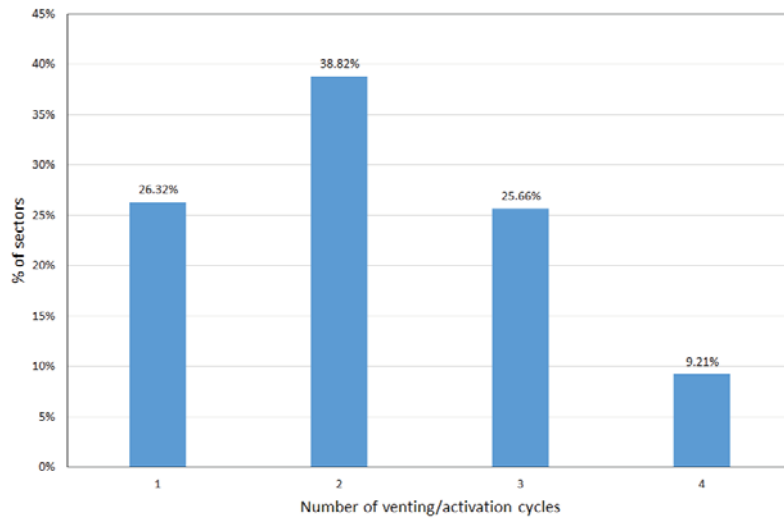
Figure 4.4: Overview of venting, bake-out and activation cycles in the LSS before LS1.
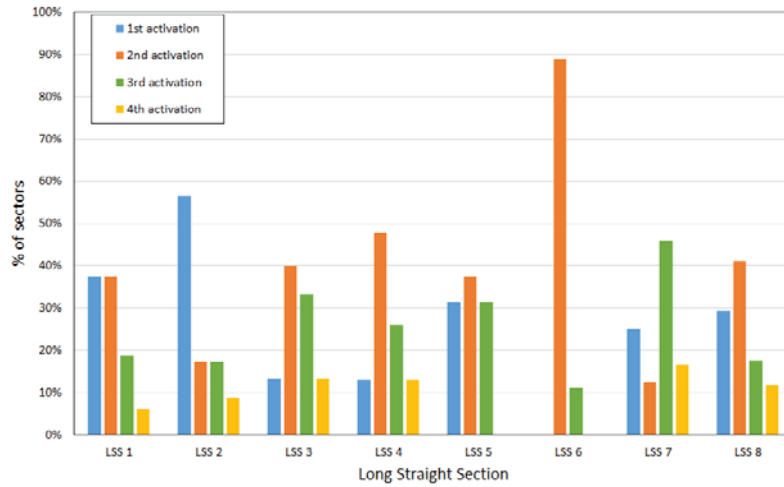
Figure 4.5: Venting, bake-out and activation cycles undergone in the LSS before LS1.

4.1.1 Vacuum system

Many interventions on the vacuum system of the LSS were performed during LS1, in order to consolidate components which showed some problems during Run 1 and to upgrade other components in order to improve their

performances.

The main interventions performed on the vacuum system during LS1 are described below:

- During the rise of beam intensity in 2011, some pressure spikes, due to beam induced sparking at RF bridges [25] of the vacuum modules, were observed. All the 1800 modules present in the LHC were subjected to X-ray analysis. The results showed that 96 RF bridges in 52 room temperature vacuum sectors were non-conform. They were thus repaired.

- During Run 1 electron clouds, due the decreasing of the bunch spacing from 150 to 25 ns, was detected. In order to minimize the impact of the pressure rise on the experiments, in 2010-11, solenoids were installed on the preferred locations for electron cloud (unbaked two-beam pipes, unbaked single beam pipes, uncoated and baked vacuum chambers). During LS1 this solution was upgraded replacing the solenoids with RF bridges made of NEG coated transition tubes.

- 88 NEG cartridges ($S_{N_2} = 400 \ \ell \cdot s^{-1}$) [19] were installed in the collimation areas (LSS 3 and 7). They were inserted in modified ion-pump vessels providing additional pumping in case of saturation of the NEG coating.

- In order to monitor the ageing of NEG material, dedicated vacuum pilot sectors were installed in LSS 2, LSS 7 and LSS 8. Here NEG cartridges are used to inject H_2 in the system by thermal outgassing.

4.2   Ultimate pressure analysis

After LS1 an analysis of the number of venting, bake-out and activation cycles undergone by each room temperature sector was carried out. Moreover the ultimate pressure, namely the lower pressure that can asymptotically be reached in a vacuum system, values in the LSS NEG coated sectors after each venting, bake-out and activation were analysed. In order to do this the

pressure values read after each cycle were collected. In a first moment the pressure values were taken just after pinch-off [15], after one week and after one month for each activation cycle. An example of pressure distribution after the first activation is shown in Figure 4.6.
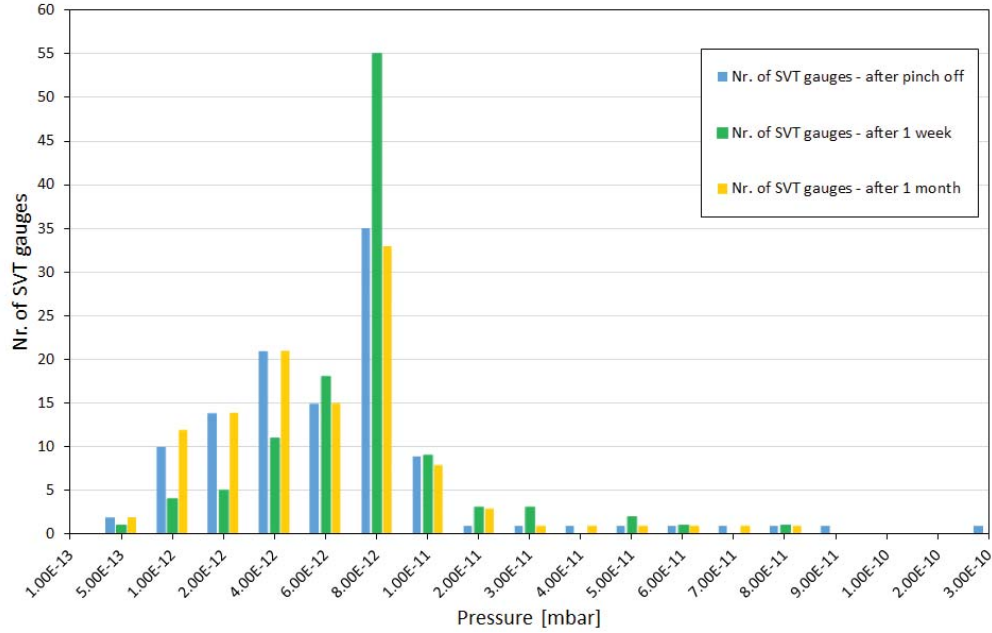

Figure 4.6: Pressure distribution after first venting, bake-out and activation cycle of all the LSS room temperature sectors.

In the next analysis just the pressure values collected one month after the activation were considered. In fact after one month the reached pressure results more stable.

The distributions (Figure 4.7) of the measured values after each cycle were so plotted in order to identify possible trends. For each distribution, a curve fitting was added and the statistical central values were considered. A clear decreasing trend of the pressures after each venting/activation cycle can be seen. A linear regression was performed on the obtained ultimate pressure statistical central values and then plotted in order to quantify the decreasing rate (Figure 4.8).
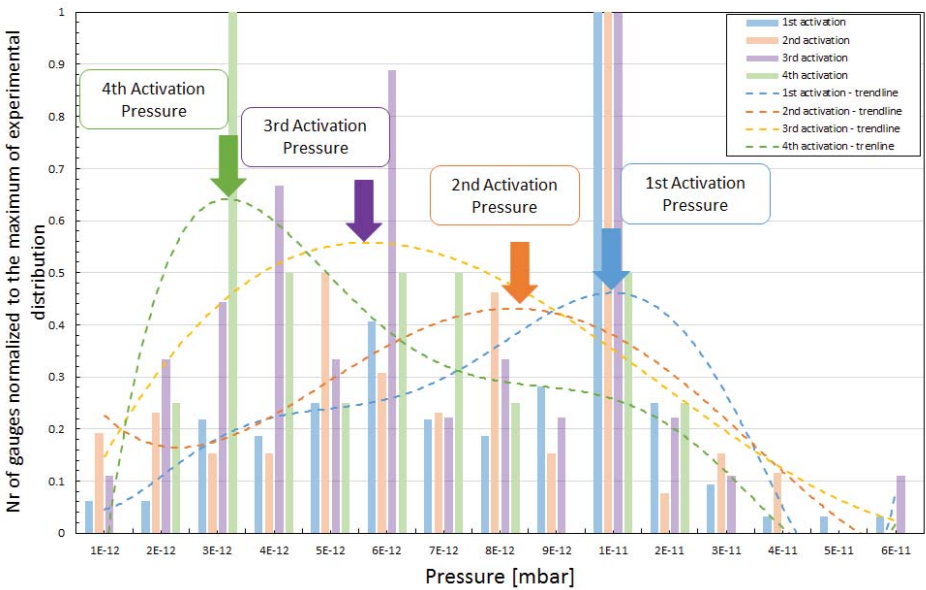
Figure 4.7: Pressure distribution one month after the end of the NEG activation.
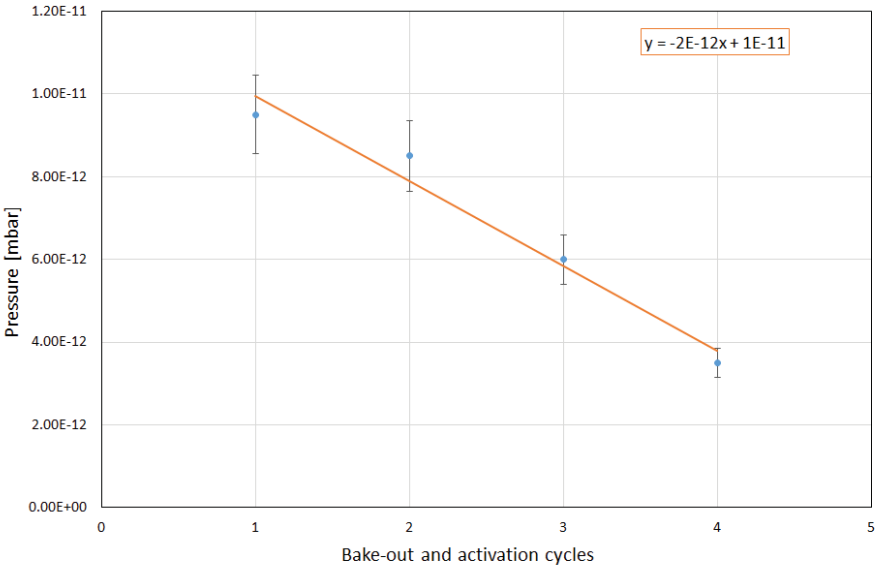
Figure 4.8: Central values of the statistical distribution of ultimate pressure in the LHC.

The pressure value measured in a NEG coated sector is the result of the combination of two quantities: the pumping speed provided by the NEG and the outgassing of the stainless steel module housing the BA gauge. To understand the pressure trend described above it was built up an experimental test bench dedicated to the study of the evolution of the NEG pumping properties after multiple venting and activation cycles.

Chapter 5

Experimental techniques

Figure 5.1: Building 113, CERN.

The aim of this work is to study the evolution of the pumping efficiency of NEG materials when subject to repeated venting, bake-out and activation cycles. In order to properly conduct the study, a dedicated experimental test

bench was built up in Building 113 (Figure 5.1) of CERN, the laboratory dedicated to vacuum characterization of the accelerators components.

5.1   Ageing Test Bench

The schematic of the test bench is shown in figure 5.2.
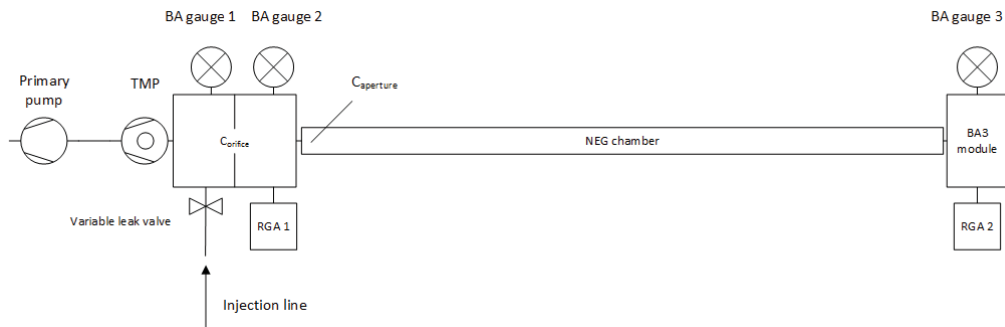
Figure 5.2: Schematic of experimental setup for ageing study on a 2.2 metres NEG coated chamber.

A 2.2 m long OFS copper of 80 mm of diameter coated with 2 μm of $TiZrV$ NEG alloy was connected to a Fischer-Mommsen type dome with a orifice of diameter $\phi = 0.87\ mm$. Pumping is provided by a Turbo Molecular Pump (Agilent Turbo V-81 M) with a nominal pumping speed for N_2 equal to $S_{N_2} = 77\ l/s$. Three Bayard-Alpert gauges are installed on the two sides of the dome and at the end of the chamber respectively. At the entrance and at the and of the chamber are installed two Residual Gas Analysers (one Balzers QMG422 with a QMA 125 head at the conductance level and one Pfiffer QMG700 at the end of the chambers). Finally, the injection line is connected to the dome by means of a Varian variable leak valve. In the line, gas bottles of H_2, CO and N_2 are installed. Pumping on the injection line is provided by another TMP, with the same characteristics of the previous one. To the injection line are connected 3 bottles of H_2, N_2 and CO, respectively.

VASCO and Molflow+ simulations were preformed in order to predict the pressure distribution along the axis of the system. It is interesting to see how the pressure profile along the NEG coated chamber assume the shape of
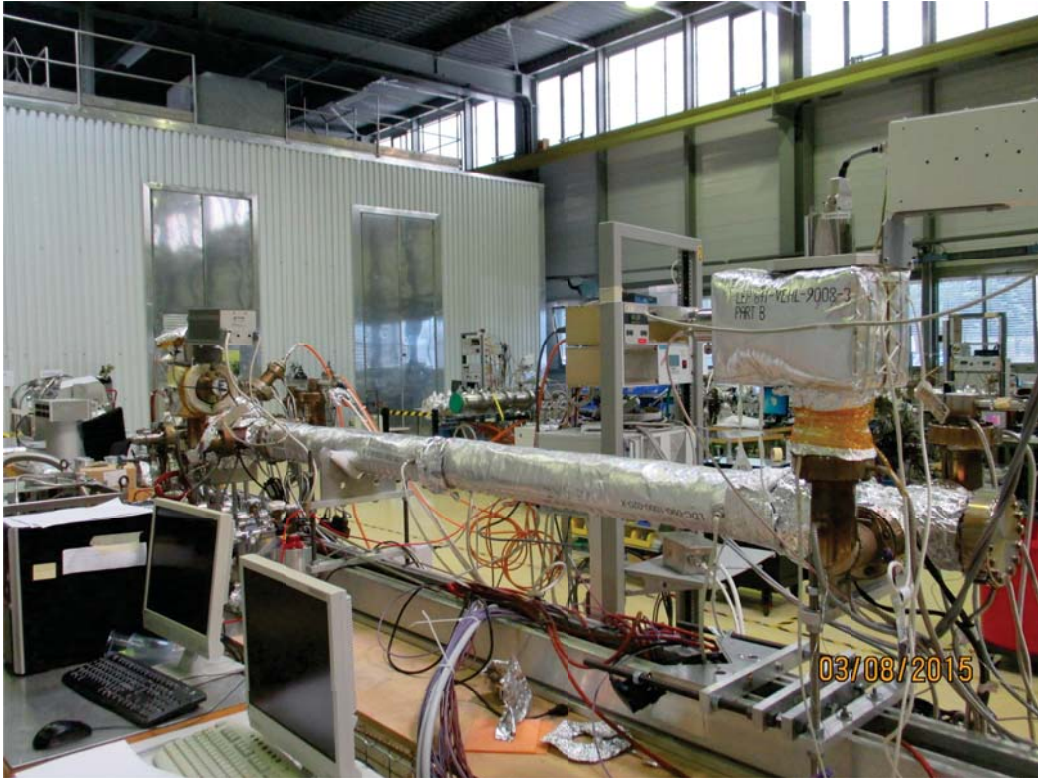
Figure 5.3: Picture of the Ageing Experimental Test Bench.

a parabola (Figure 5.5). It is due to the fact that on the extremities of the chamber are installed stainless steel modules housing the BA gauges, whose outgassing rate causes a pressure increase.

The characterization of the evolution of NEG performances was brought out repeating the same procedure for fifteen times. The procedure was divided in 3 main steps: venting, bake-out, activation and finally gas injections. The venting of the system was provided connecting a N_2 45 (99.995% pure) bottle on a variable leak valve. Before venting the system, the valve connecting the TMP to the vacuum system is closed; at this point the bottle, and then the variable leak valve, are opened in order to allow N_2 to flow into the system. The pressure difference between the vacuum system and the outlet of the bottle is monitored through a differential manometer, which allow to know the pressure injected into the chamber (1 bar in this study).
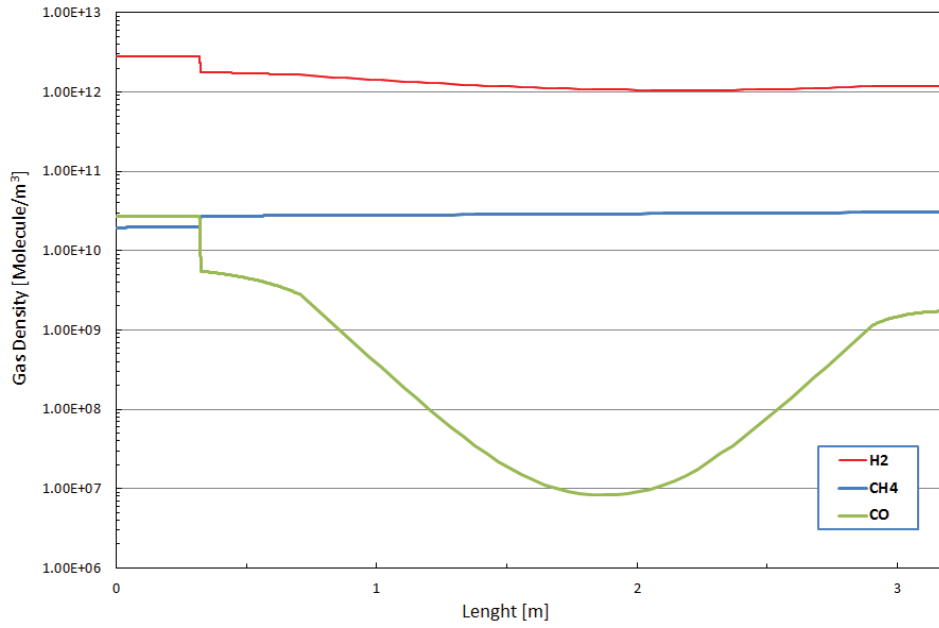
Figure 5.4: Gas density distribution resulting from VASCO simulation.
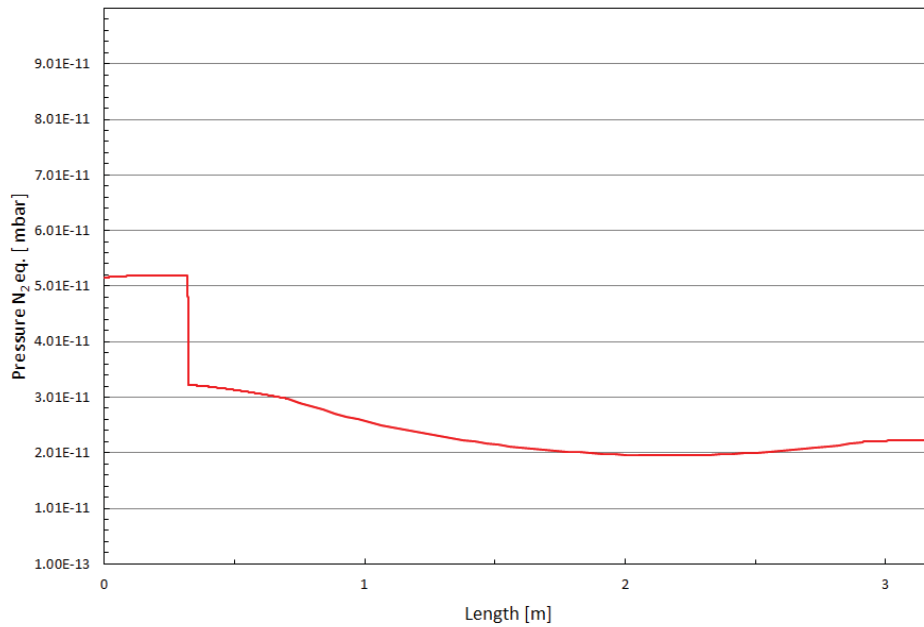
Figure 5.5: Pressure distribution resulting from VASCO simulation.

<center>(a)</center>

<center>(b)</center>
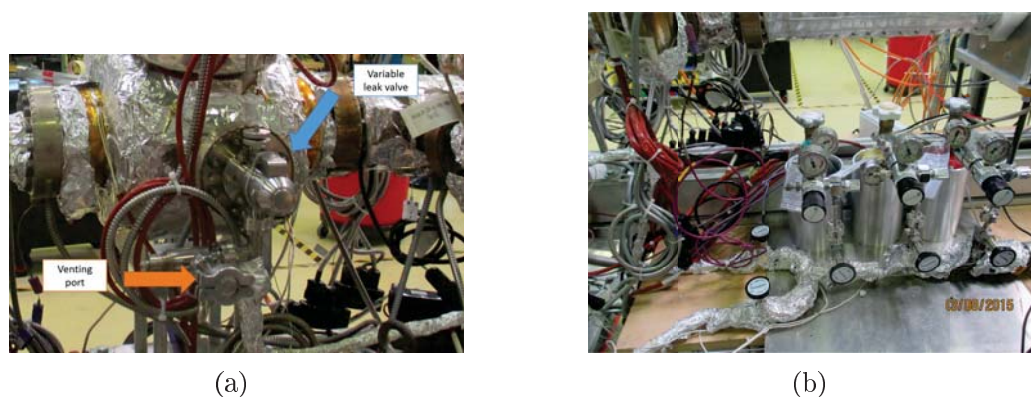
Figure 5.6: The connection system between the injection line and the vacuum system (a) with the ISO-KF DN25 flange dedicated to venting. In (b) it is shown the injection table connected to the line.

Figure 5.6 shows some details of the injection line and of the venting port. Downstream the ISO-KN DN25 there is a valve to allow the connection of the N_2 bottle to the system. When the pressure of 1 bar is reached the variable leak valve is closed and the system is left in static condition (without pumping), for 10-12 hours. Afterwards the TMP valve is re-opened to start the pumpdown.

When pressure values in the order of 10^{-8}-10^{-9} mbar are reached the bake-out of the system can be started.

The bake-out is made following different procedures depending on the type of component. Five different programs were created to bake the system (Figure 5.7).

After the cool down it's necessary to wait at least 24 hours to reach the ultimate pressure value. After that time it is possible to begin with the gas injections. In order to minimize the contamination during the injection, a procedure called *flush* is performed on the injection line. The flush procedure is schematically explained in Figure 5.8.

	Steps	1	2	3
Program 1: NEG Coated Parts	Ramp rate[°C/h]	50	60	80
	Max Temp. [°C]	120	230	20
	Plateau duration [h]	24	24	24
Program 2: Stainless Steels and Penning gauge	Steps	1	2	3
	Ramp rate[°C/h]	75	80	100
	Max Temp. [°C]	250	150	20
	Plateau duration [h]	24	24	24
Program 3: Injection line	Steps	1	2	3
	Ramp rate[°C/h]	50	50	80
	Max Temp. [°C]	180	180	20
	Plateau duration [h]	24	24	24
Program 4: TMP and valves	Steps	1	2	3
	Ramp rate[°C/h]	50	50	100
	Max Temp. [°C]	140	140	20
	Plateau duration [h]	24	24	24
Program 5: RGA + SVT Gauges	Steps	1	2	3
	Ramp rate[°C/h]	75	100	60
	Max Temp. [°C]	350	180	20
	Plateau duration [h]	24	24	24

Figure 5.7: Bake-out programs for different components of the system.

After the flush, the last sector of the injection line downstream the variable leak valve is filled with 50 mbar and isolated from the rest of the injection line. The injection can thus be started. The amount of gas entering the system can be controlled regulating the aperture of the variable leak valve. The pressure rise during the injection is followed on the 3 BA gauges and the 2 RGAs installed on the system and recorded by mean of dedicated software. H_2, N_2 and CO are injected into the system. Before each injection the system is pumped down (6 hours) until the base pressure is reached again. A first analysis of the collected data allows to determine if the injections were properly done or if they need to be repeated. In the former case the system is vented and all the cycle is restarted form the beginning, in the latter the injection are performed again before to vent the system. With the data re-

(a)

(b)
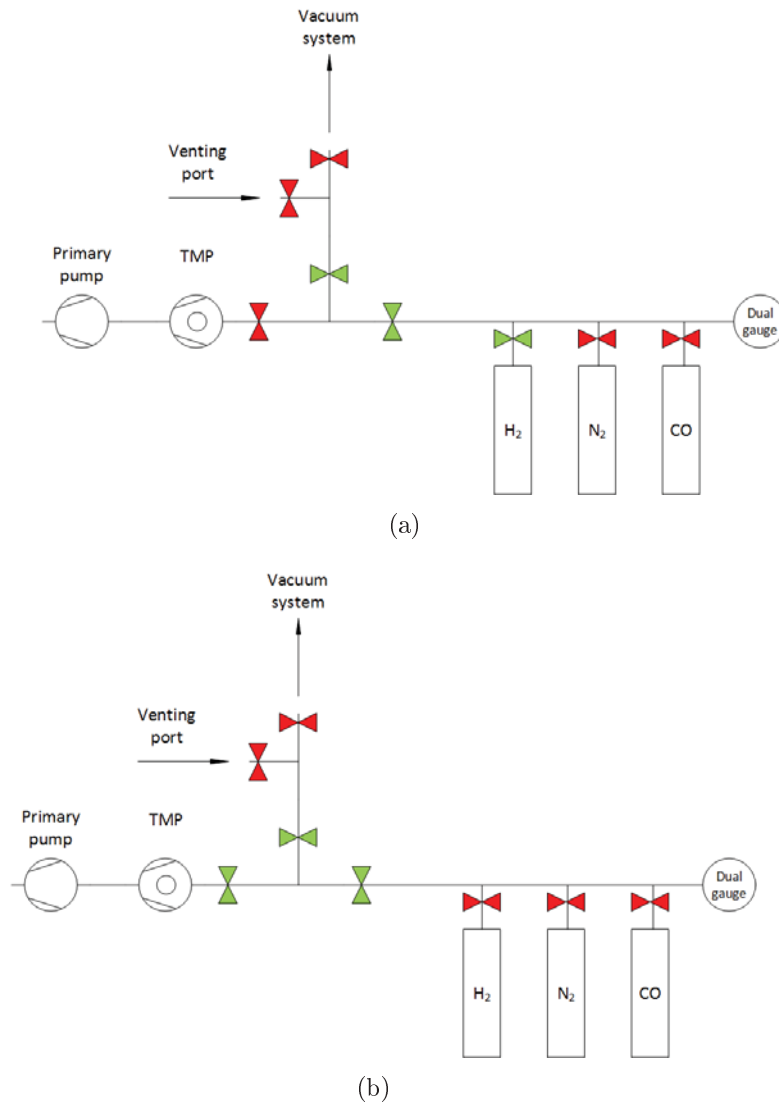
Figure 5.8: Schematic of the injection line and of the valve configuration for first (a) and second (b) step for the flush of the (before H_2 injection in this example).

sulting from each measurement it was possible to calculate the parameters for the characterization of the vacuum chamber, namely total transmission (Tr_{tot}), partial transmission (Tr_{par}), pumping speed (S), capture probability (CP) and the outgassing rate (Q_{end}) of the module at the end of the chamber housing BA_3 gauges and RGA_2, for every injection. The definition of the four parameters for the system is given in Table 5.1.

Table 5.1: Definition of the quantities used for characterization of Ageing Test Bench

S_{NEG}	Tr	$CP\%$	Q_{end}
$\dfrac{Q}{P_{BA_2}} = \dfrac{C(P_{BA1}-P_{BA2})}{P_{BA2}}$	$\dfrac{\Delta P_{BA2}}{\Delta P_{BA3}}$	$\dfrac{S_{NEG}}{C_{Aperture}}$	$S_{NEG}P_{BA3}$

Transmissions and capture probability were used to calculate the sticking factor s entering them in the Tr-s and in the CP-s curves (Figure 5.9 and 5.10) respectively.
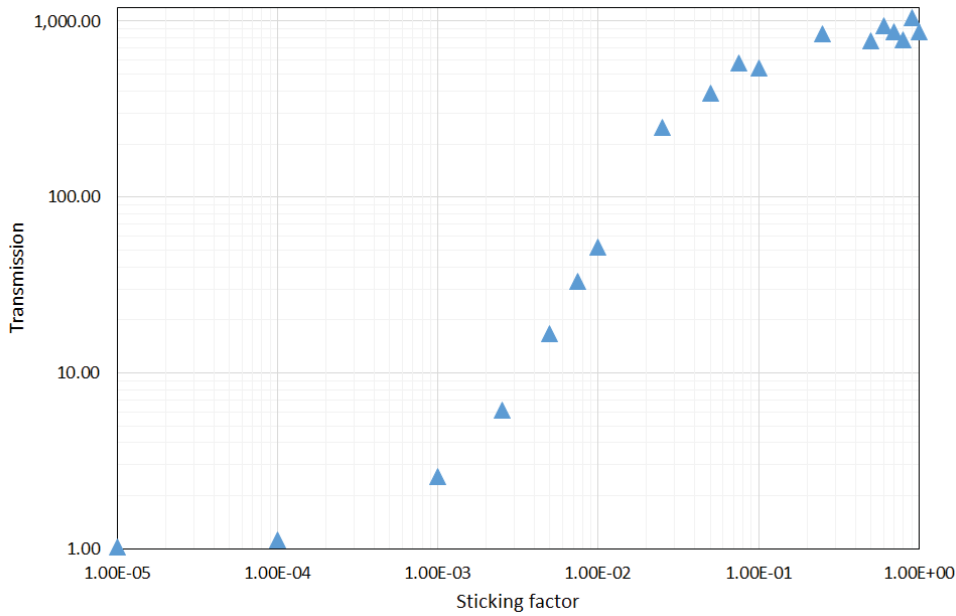
Figure 5.9: Transmission-sticking factor curve calculated by Molflow+ simulations.

The conductance ($C_{orifice}$) of the orifice ($\varphi = 8.7$ mm) in the Fischer-Mommsen type dome and of the aperture of the NEG chamber ($C_{aperture}$) were calculated for the injected gases (Table 5.2).

The Capture Probability was finally not used for the determination of the sticking factor. The reason is that the slope of the CP-s curve is too low, implying that a small variation in the CP corresponds to an important variation of s, making the resulting s values not reliable.
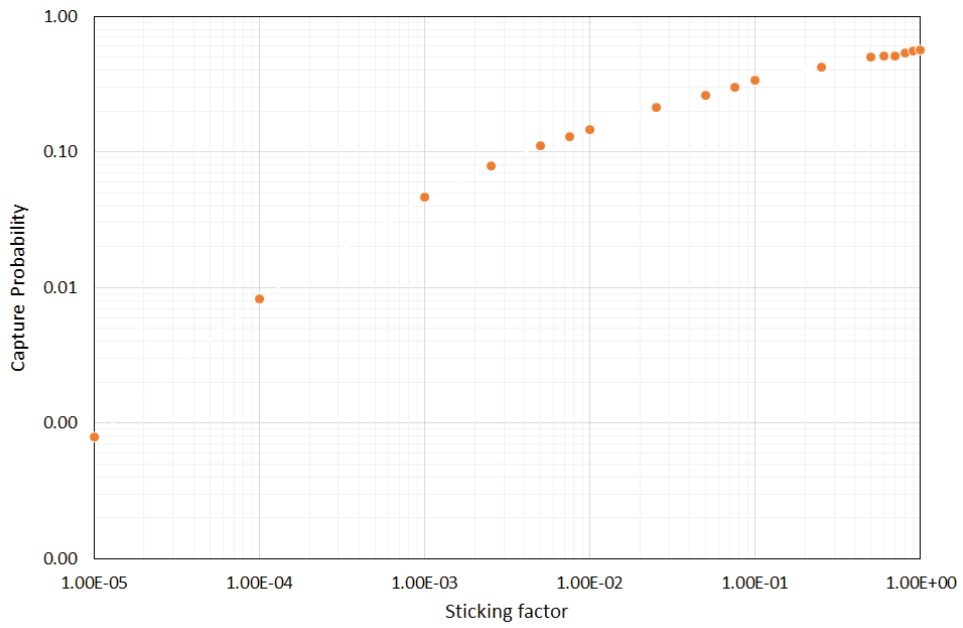
Figure 5.10: Capture Probability-Sticking factor curve calculated by Molflow+ simulations.

Table 5.2: Conductance of the orifice into Fischer-Mommsen dome and of the aperture of the NEG chamber.

	H_2	N_2	CO
$C_{orifice}$	23.9	6.4	6.4
$C_{aperture}$	2219.3	593.1	593.1

5.2   NEG Pilot Sector
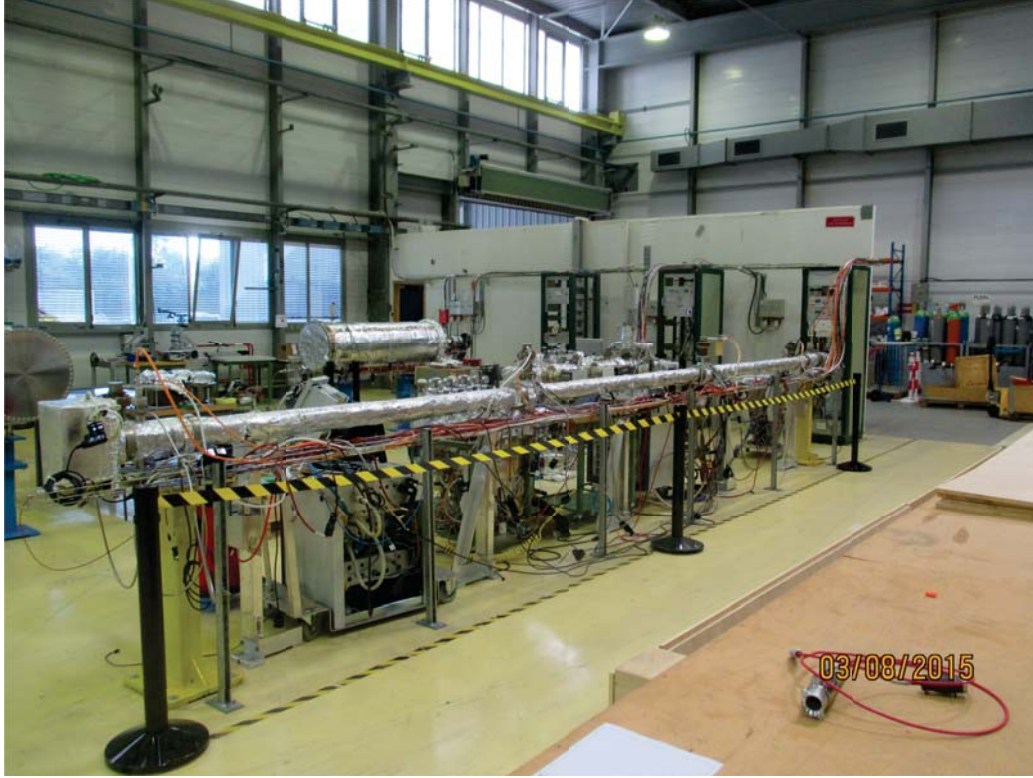
Figure 5.11: Picture of a copy of the NEG pilot sector.

The NEG Pilot sector is a system installed in six different point of the LCH tunnel (specifically in sectors A5R2.B, A5R2.R, IP7.B, IP7.R, A6L8.B and A6L8.R). It was designed to regularly evaluate the level of saturation of the NEG coating in order to ensure the required average pressure during the operation with beams. The evaluation of the performances of the NEG is achieved using the transmission method. The H_2 injection are performed by thermal outgassing of a NEG cartridge installed under one of the two central modules of the system. A technical drawing of the NEG pilot sector is presented in Figure 5.12. The two modules hosing the BA gauges are made of stainless steel and totally NEG coated. For impedance reason, RF screens are welded at each port of the modules. At the gauge port, as shown in Figure 5.13, in order to intercept possibly scattered particles, like photons,

electrons or protons, thereby minimising the background to the instruments,
two baffles with half-moon shape are installed behind the RF screen inside the
instrumented transitions. The BA modules connect three 2.2 meters NEG
coated chambers identical to the one installed on the Ageing Test Bench.
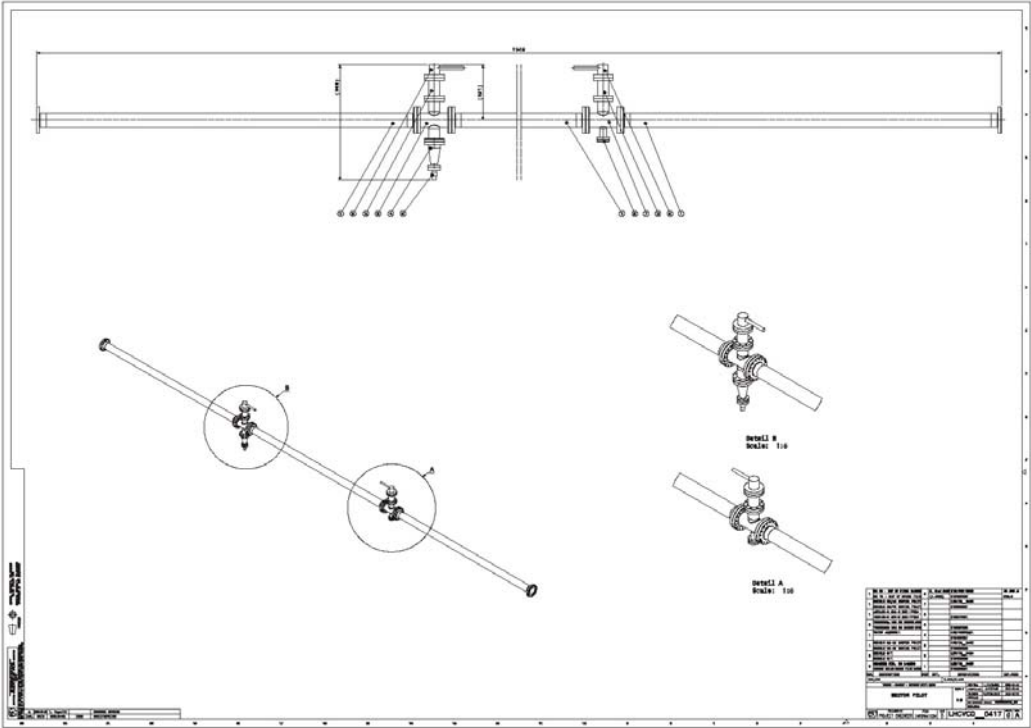
Figure 5.12: Technical drawing of NEG pilot sector.

Figure 5.13: Half-moon baffles installed at the gauge port.

Transmission was measured injecting H_2 by mean of a NEG cartridge (CapaciTorr D400, SAES-Getters). A schematic of a NEG cartridge is shown in Figure 5.14. It is composed by NEG sintered disks to provide the pumping and a heater to activate the NEG. The activation is provided heating the cartridge at 450°C (5 A) for 45 minutes. By heating the cartridge at lower temperature it is also possible to preform H_2 injections; according to Sievert's law, the dissociation pressure decreases increasing the temperature of the material, thus enhancing H_2 outgassing.
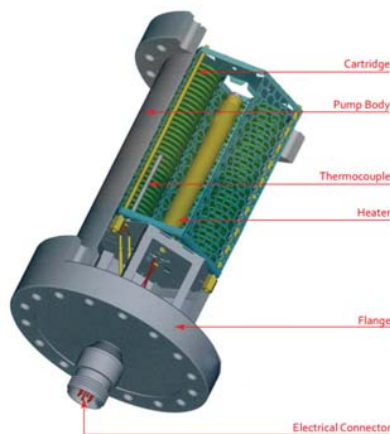
Figure 5.14: Schematic of a NEG cartridge.

In this study the injections were performed with a current of 4 A, corresponding to a temperature of 400°C. Figure 5.15 indicates the expected H_2 pressure, at the BA gauge in front of the cartridge, as a function of the current applied to the power supply.
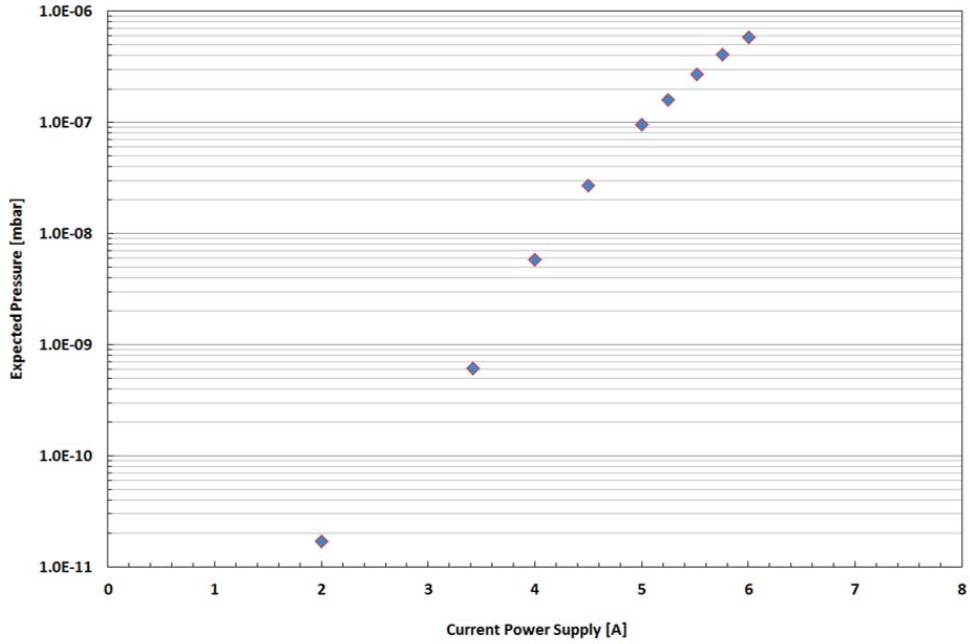
Figure 5.15: Injection in NEG pilot sector.

The injection and the pressure follow up are made in remote, so it's not necessary to access to the LHC tunnel. An example of the results of an H_2 injection is shown in Figure 5.16.

The sticking factor was calculated using the Transmission method. Molflow+ simulations of the chamber were performed. It is important, while setting the parameters of the simulation, to take into account that the NEG cartridge, when not used for injections, is a pump, which provide a pumping speed $S_{H_2} = 400\ell \cdot s^-1$. The resulting Tr-s curve is shown in Figure 5.17.
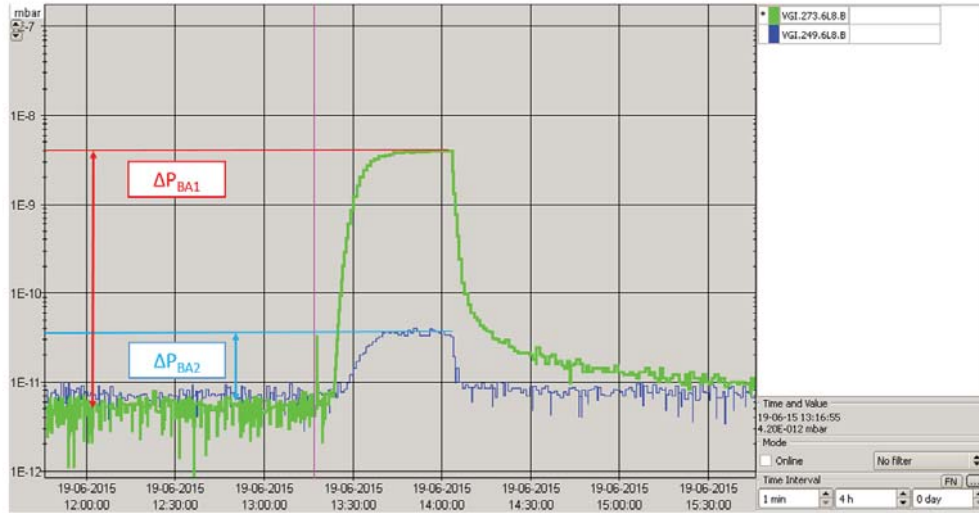
Figure 5.16: Injection in NEG pilot sector.
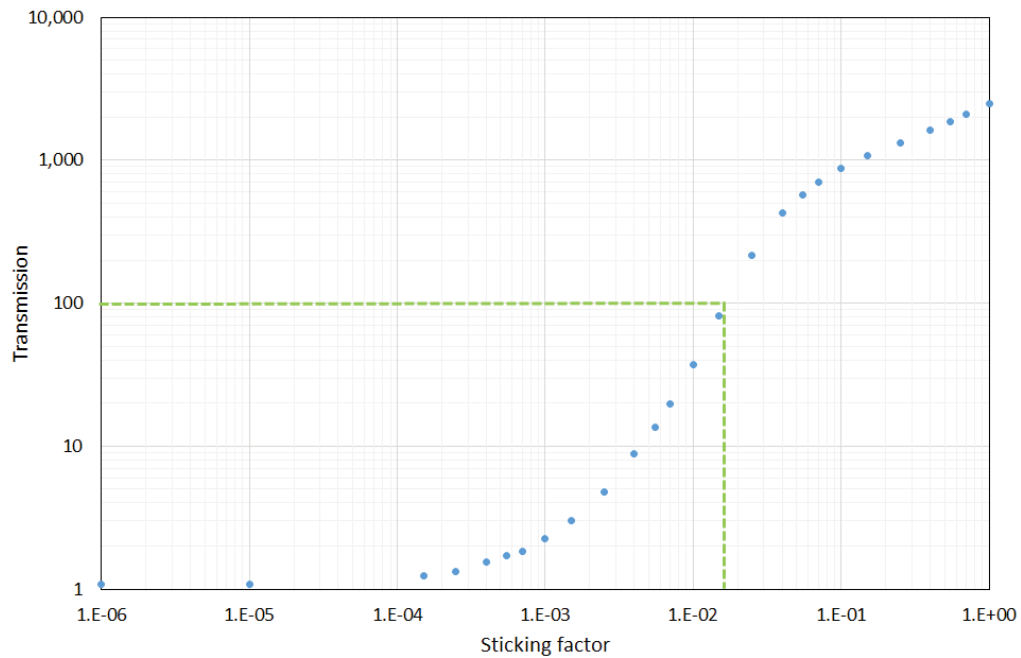
Figure 5.17: Tr-s curve for the NEG Pilot Sector.

Chapter 6

Results

6.1 Ageing Test Bench

The analysis of the data obtained after 15 venting, bake-out and activation cycles on the Ageing Test Bench in Building 113 is here presented.

6.1.1 Sticking factor analysis

The sticking factor obtained by Tr_{tot} and Tr_{par} are plotted in Figure 6.1 and 6.2 respectively.

In both cases, a clear decrease of the sticking probabilities after each activation cycle can be seen. In case of H_2, the two curves of Fig. 6.1 and 6.2 are quite similar; this indicates that either total or partial pressure can be used for the sticking probability measurement. For N_2 the two curves appear slightly different. The difference is even more obvious in the case of CO, for which the ratio between the slopes of the curves differs by a factor of 2. The discrepancy between the two curves is due to the free transmission of gas species that are not pumped by the NEG film, such as CH_4, Ar and He. The rare gas can be a contamination in the injected gas. CH_4 can also be produced in the instruments, possibly due to H_2 interaction with the hot filaments of the BA gauge. The higher the sticking probability for the injected gas, the smaller the amount of that gas that reaches the end of the chamber. As a consequence, the non-pumped gas has an increased
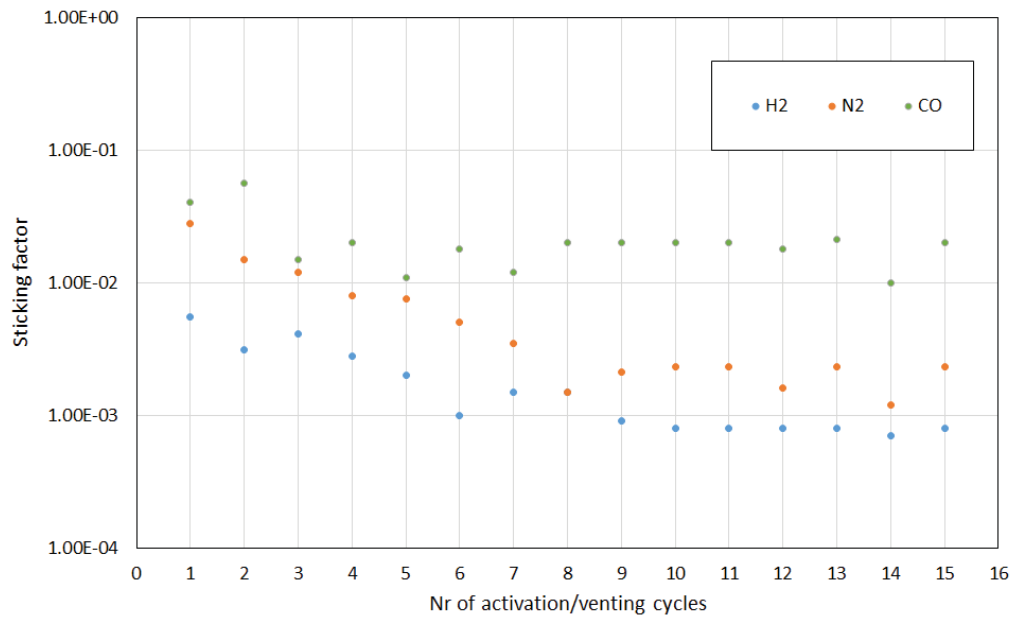
Figure 6.1: Sticking factor obtained using total pressure transmission.
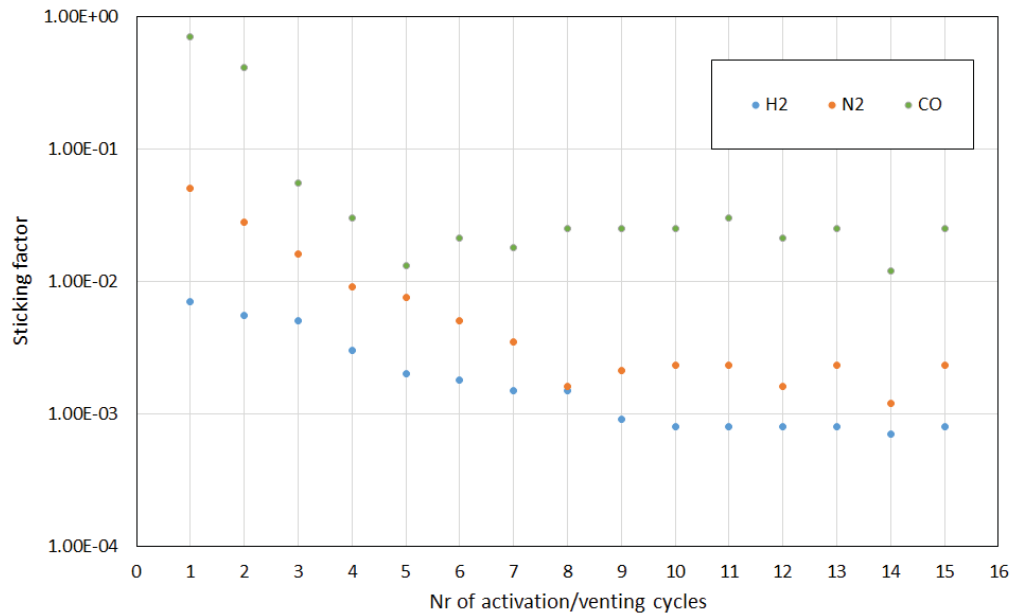
Figure 6.2: Sticking factor obtained using partial pressure transmission.

contribution to the total pressure reading at the extremity of the vacuum chamber: the total pressure ratio is not anymore correlated with the sticking probability of the injected gas (s is underestimated). This implies that for N_2 and CO the partial pressure ratio has to be used to evaluate the sticking probability. Figure 6.3 shows the average gas composition as seen by RGA_2, at the of the chamber, measured during the last injection step. For CO just the 30% of pressure rise is due to CO itself, explaining the big difference in slope between Figure 6.1 and Figure 6.2.
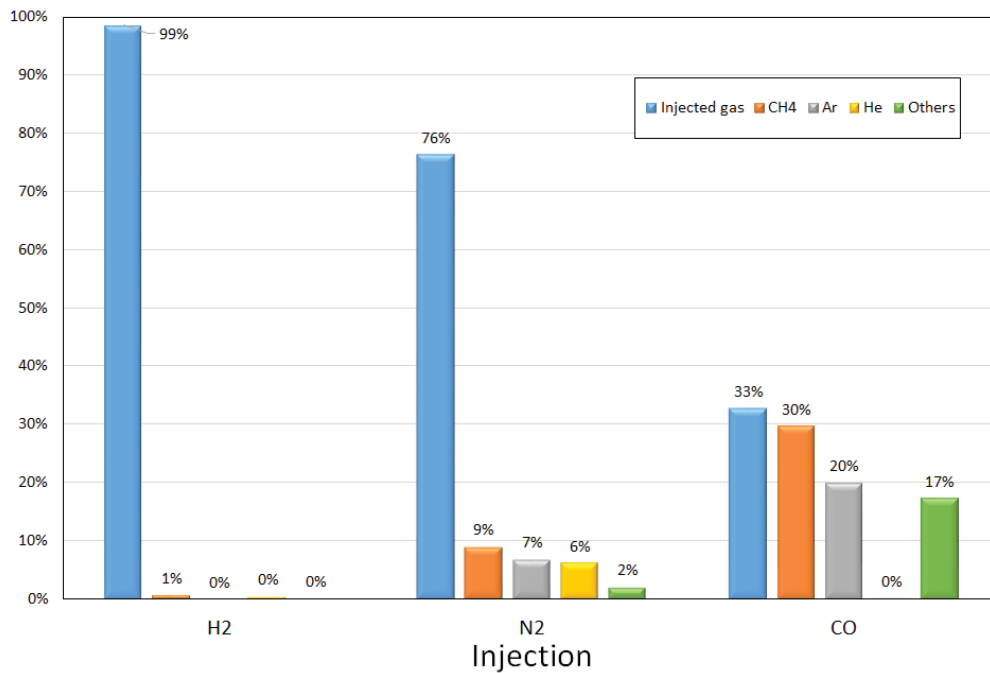
Figure 6.3: Average gas composition at last step of different gas injections as seen by RGA_2 at the end of the chamber.

Limits in the application of the transmission method

The simulations performed with Molflow+ showed that the sticking probability strongly depends on the geometry of the chamber in which the injection in performed. For cylindrical pipes geometrical parameters are the length L and the radius R of the pipe. Figure 6.4 shows the Tr-s curves for different L/R.
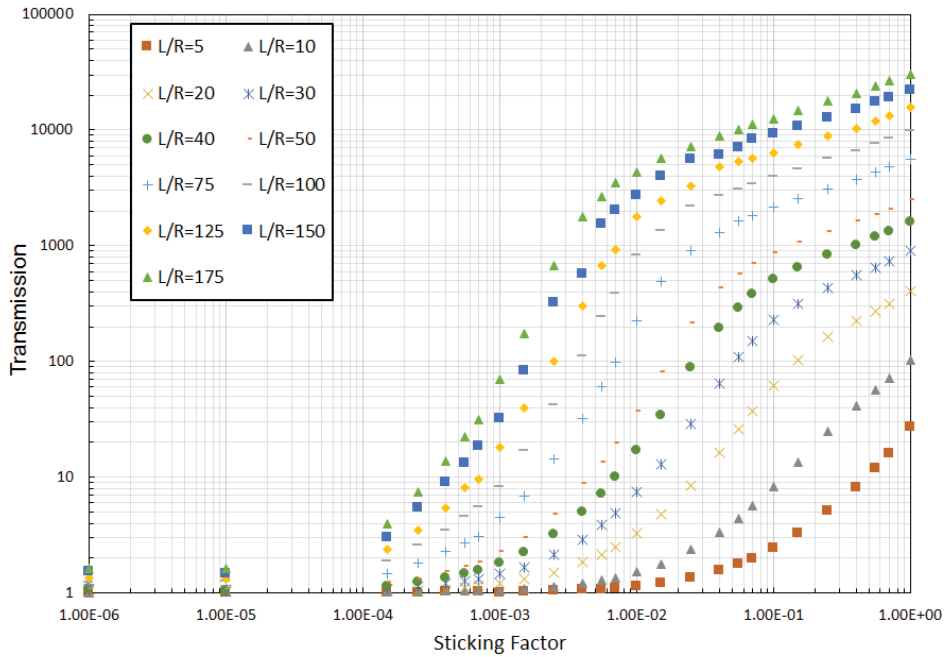
Figure 6.4: Tr-s curves for different L/R values.

When L/R grows, to higher transmission correspond lower sticking factor values.
In order to estimate the sticking factor with acceptable precision, the transmission value must be in a range corresponding to the steepest part of the curve, otherwise a small error in the transmission measurement (for instance due to the intrinsic error of the BA gauge) can bring to a big error in the estimation of the sticking factor.

Table 6.1: Sticking factor ranges for H_2, N_2 and CO.

	Sticking factor
H_2	$7.0 \cdot 10^{-3}$ - $7.0 \cdot 10^{-4}$
N_2	$5.0 \cdot 10^{-2}$ - $1.2 \cdot 10^{-3}$
CO	$7.0 \cdot 10^{-1}$ - $1.2 \cdot 10^{-2}$

In Table 6.1 are listed the sticking factor ranges for H_2, N_2 and CO (taken by Figure 6.1). The values covers a total range of almost four order of magnitudes, and so all possible slopes of the curves in 6.4.
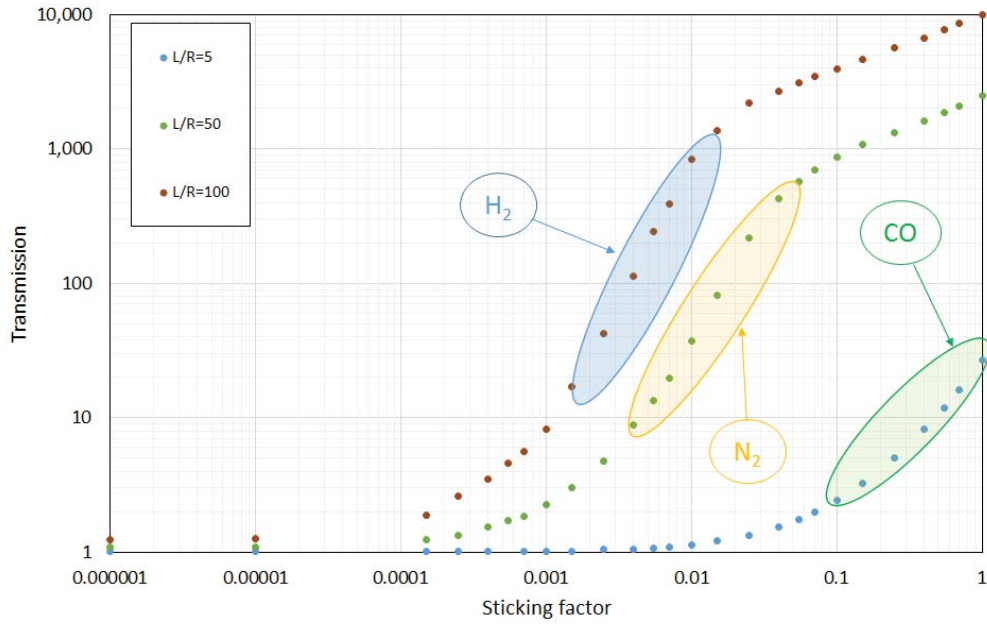
Figure 6.5: Tr-s curves for different L/R values.

Thanks to the different sticking factors related to H_2, N_2 and CO it is possible to perform an accurate characterization of NEG coated chambers of any geometry, just selecting the right gas for the injection.
As shown in Figure 6.5, progressively increasing L/R, CO, N_2 and finally H_2 have to be used.

Outgassing of the BA modules

The decrease of the outgassing rate of the stainless steel modules housing the BA gauges can affect the evaluation of the transmission values and thus of the sticking factor. Therefore the outgassing (Q_{BA3}) of the BA_3 module was calculated for every injection, in order to put in evidence possible trend and correct the transmission values. Q_{BA3} is thus given by:

$$Q_{BA3} = S_{NEG}P_{BA3,bi} \qquad (6.1)$$

The results are shown in Figure 6.6.
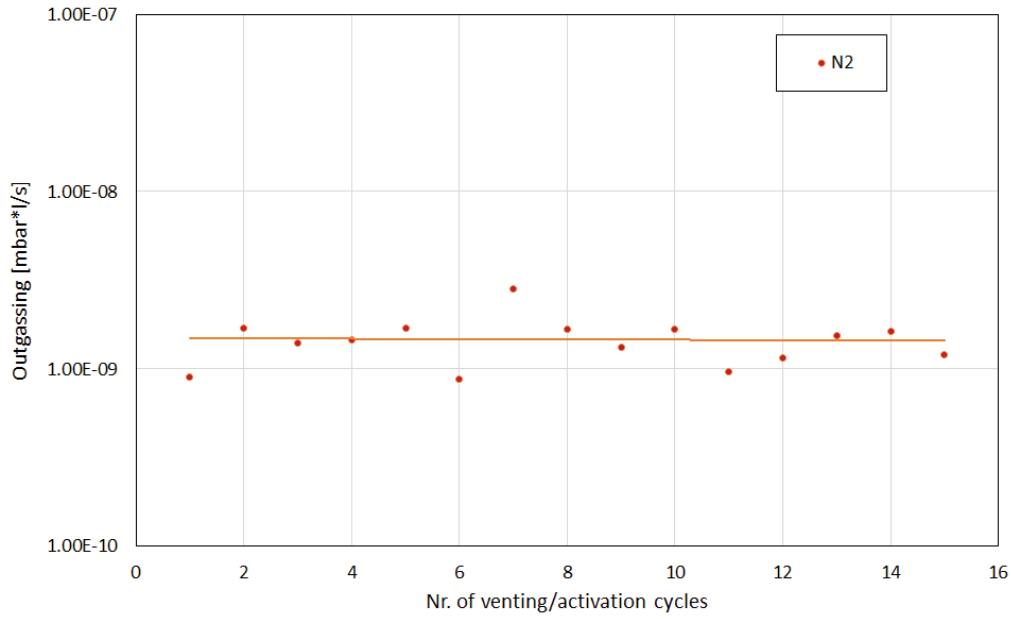
Figure 6.6: BA_3 gauge outgassing calculated by pumping speed values during N_2 injection.

It is possible to see in Figure 6.6 that the outgassing values are constant and scattered around the average value of $3 \cdot 10^{-9}$. The scatter is due to BA gauge measurement intrinsic error and to $P_{BA3,bi}$ scatter depending on the time passed between the end of the activation and the beginning of the injection. Considering that the outgassing is constant, it doesn't affect the study of the evolution of the transmission values.

6.1.2   Pumping speed

The analysis of the NEG pumping speed after each venting, bake-out and activation had the final aim to explain the pressure behaviour in the LHC seen in 4.2.

Figure 6.7 shows the pumping speed evolution for each injected gas.
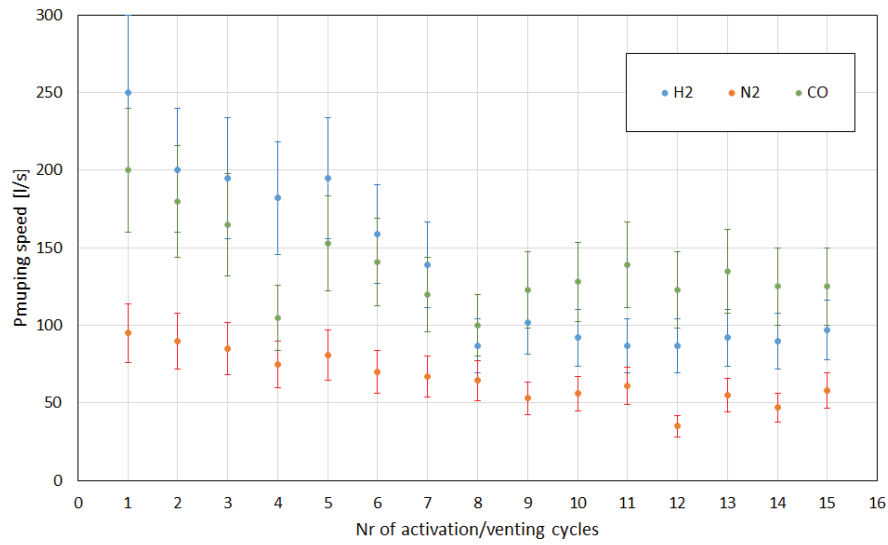
Figure 6.7: Pumping speed values.

The curve shows a decreasing trend. Every time that the NEG is activated the oxygen on the surface diffuses into the bulk. Thus after every venting and activation cycle the oxygen concentration inside the film increases of a non-negligible amount [6]. This saturation process is the most probable cause of the pumping speed decrease shown in Figure 6.7. The specific data of the pumping speed values are shown in Table 6.2. They were calculated, like transmissions, considering the quantities at the last injection step. the error bars take into account the error ($\pm 20\%$ [21]) due to the measurement uncertainty of the BA gauges. The pumping speed decreases of a factor of about 1.1 after each venting, bake-out and activation cycle.

Table 6.2: Pumping speed experimental values.

Nr. of venting/activation	S_{H_2}	S_{N_2}	S_{CO}
1	250	95	200
2	200	90	180
3	195	85	165
4	182	75	105
5	195	81	153
6	159	70	141
7	139	67	120
8	87	65	100
9	102	53	123
10	92	56	128
11	87	61	139
12	87	35	123
13	92	55	135
14	90	47	125
15	97	58	125

6.1.3   LHC pressure long term analysis

Using the average pressure values in the LHC estimated in 4.2 and the pumping speed measured on the test bench, it is possible to make a prediction of the evolution of the pressure values in the LHC after 15 venting, bake-out and activation cycles. The procedure used for the data analysis is explained below.
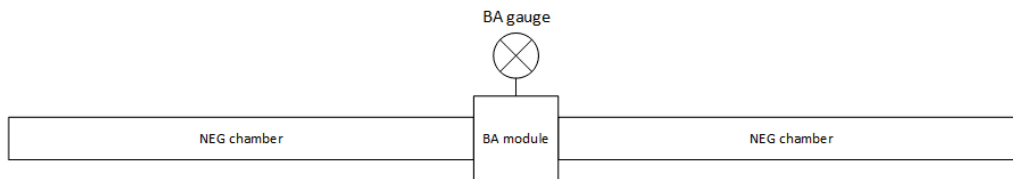
Figure 6.8: Schematic of LSS sector model.

The schematic of the model used to describe an LHC LSS sector is shown in Figure 6.8.

Considering that the module in Figure 6.8 is connected to two NEG chambers, the pumping speed $S_{NEG} = 2S_{H_2}$. The considered variables are the pressure measured on the BA gauge, the pumping speed provided by the two NEG chambers and the outgassing of the module housing the BA gauge.

Table 6.3: Calculated outgassing of a BA stainless steel.

Nr. of venting/activation	S_{NEG}	$P_{meas,LHC}$	Q_{module}
1	500	$9.5 \cdot 10^{-12}$	$4.75 \cdot 10^{-9}$
2	400	$8 \cdot 10^{-12}$	$3.4 \cdot 10^{-9}$
3	390	$6 \cdot 10^{-12}$	$2.3 \cdot 10^{-9}$
4	364	$3.5 \cdot 10^{-12}$	$1.3 \cdot 10^{-9}$

The first step was to calculate the outgassing of the module Q_{mod} using the average values of pressure $P_{meas,LHC}$ and the pumping speed values measured on the Ageing Test Bench (Table 6.3). Considering that H_2 outgassing and pumping is the dominant phenomenon in the LSS, just S_{H_2} is taken into account. Curve fitting on the outgassing data was then performed (Figure 6.9). A decreasing exponential function was chosen taking into account the results about outgassing trend made in other studies [9]. Using the exponential function so found, the outgassing values for the cycles going from the 5th to the 15th were calculated.
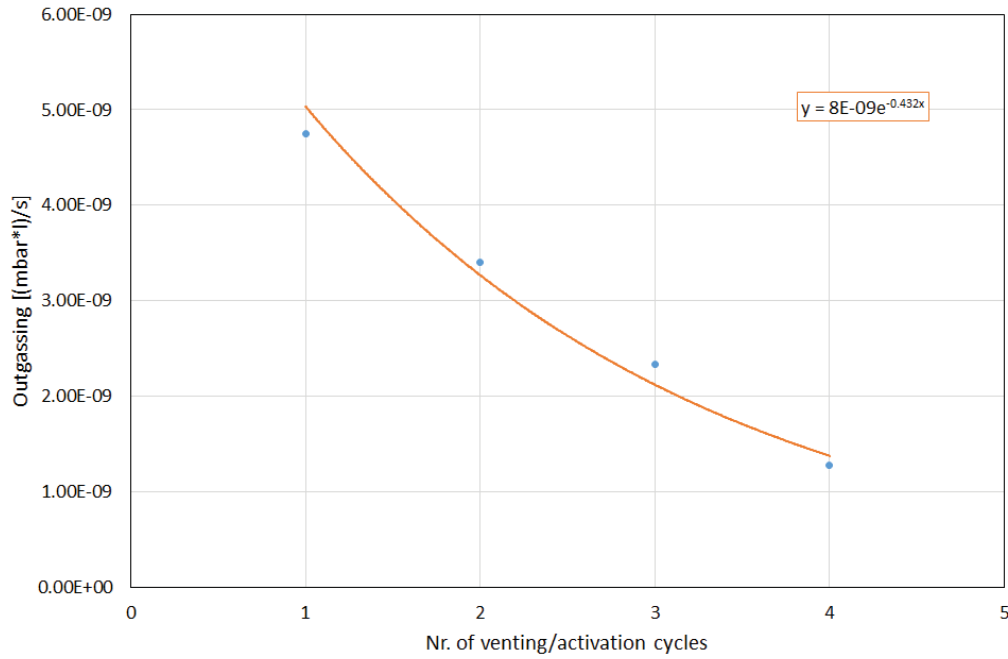
Figure 6.9: Evolution and curve fitting of the calculated outgassing af BA gauge module.

The last step was to combine the calculated outgassing Q_{calc} data with the S_{NEG} measured on Ageing Test Bench in order to obtain the expected pressure $P_{expected}$ in the LSS after 15 cycles of venting, bake-out and activation. The results are summarized in Table 6.4 and in Figure 6.10.

Table 6.4: Summary of the expected pressure in the LHC.

Nr. of venting/activation	$S_N EG$	Q_{calc}	$P_{expected}$
5	390	$9.23 \cdot 10^{-10}$	$2.37 \cdot 10^{-12}$
6	318	$5.99 \cdot 10^{-10}$	$1.88 \cdot 10^{-12}$
7	278	$3.89 \cdot 10^{-10}$	$1.40 \cdot 10^{-12}$
8	174	$2.52 \cdot 10^{-10}$	$1.45 \cdot 10^{-12}$
9	204	$1.64 \cdot 10^{-10}$	$8.03 \cdot 10^{-13}$
10	184	$1.06 \cdot 10^{-10}$	$5.78 \cdot 10^{-13}$
11	174	$6.91 \cdot 10^{-11}$	$3.97 \cdot 10^{-13}$
12	174	$4.48 \cdot 10^{-11}$	$2.58 \cdot 10^{-13}$
13	184	$2.91 \cdot 10^{-11}$	$1.58 \cdot 10^{-13}$
14	180	$1.89 \cdot 10^{-11}$	$1.05 \cdot 10^{-13}$
15	194	$1.23 \cdot 10^{-11}$	$6.32 \cdot 10^{-14}$
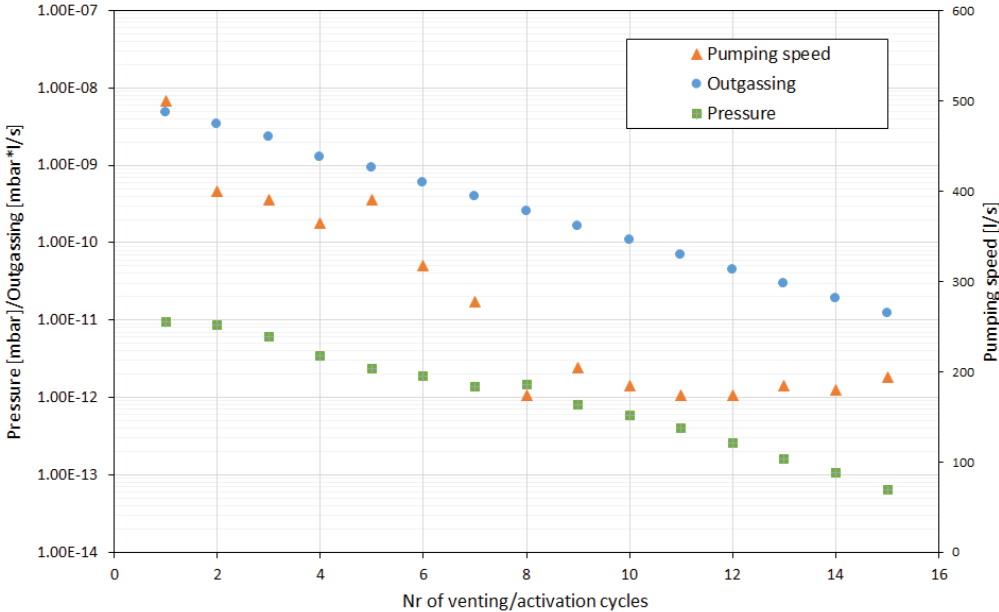
Figure 6.10: Summary of the predicted values of outgassing, pumping speed and resulting pressure in the LSS of the LHC.

In figure Figure 6.10 a decreasing trend for the pressure is clear. The ratio between a pressure values and the next one is constant and equal to 1.42.

6.2   NEG Pilot Sector

Dynamic effects of the beam, such as photon, ion and electron stimulated desorption [10], cause a pressure increase in the LHC during operations. As a consequence, considering the induced gas load, NEG is saturated faster than in static vacuum conditions. The NEG Pilot Sector was designed to measure the saturation of NEG due to beam dynamic effects.

Collecting the transmission values during the technical stop it will be possible to define a trend of the sticking factor values. Considering that the NEG pilot sectors were installed during LS1, since now just two injections have been performed on the system. The results are listed in Table 6.5 and Table 6.6.

Table 6.5: Sticking factor calculated after the injection of the 19/05/2015.

Sector	Red line	Blue line
A6L8	$1.5 \cdot 10^{-2}$	$1 \cdot 10^{-2}$
IP7	$3 \cdot 10^{-2}$	$1.5 \cdot 10^{-2}$
A5R2	$1.2 \cdot 10^{-2}$	$1.2 \cdot 10^{-2}$

Table 6.6: Sticking factor calculated after the injection of the 19/06/2015.

Sector	Red line	Blue line
A6L8	$1.8 \cdot 10^{-2}$	$1 \cdot 10^{-2}$
IP7	$2.5 \cdot 10^{-2}$	$2 \cdot 10^{-2}$
A5R2	$2 \cdot 10^{-2}$	$2 \cdot 10^{-2}$

The gas load induced by the beam dynamic effects is much smaller then the one due to venting or gas injections. Therefore the NEG saturation caused by those effects is a slow process, thus it will take a time in the order of years to observe appreciable variation of the NEG performances.

Chapter 7

Conclusions

During Run 1 of the LHC the design vacuum requirement were totally fulfilled, confirming the absolute reliability of NEG coating as a pump. However during LS1 most of the chambers were opened to allow the interventions and so needing a new activation.

In order to properly plan Long Shutdown 2 and 3, it is of primary importance to fully understand how the performances of NEG materials change after a considerable number of venting, bake-out and activation cycles. An analysis of the ultimate pressure values in the LHC was performed to summarize the vacuum performances in the machine. This analysis pointed out a decreasing trend of the average pressure values. In order to explain this trend and to study in detail the evolution of the pumping performances of NEG, part of this work was conducted in Building 113 at CERN, on a dedicated experimental test bench. Here a 2.2 metres NEG coated chamber was vented, baked and activated fifteen times. Through total and partial pressure transmission measurements, sticking factor, capture probability and pumping speed were estimated.

During the experimental activity important results concerning the accuracy and the reliability of the characterization methods were carried out. The precision of the transmission method showed its strong dependence on the geometry of the system. To overcome this limit it was observed that, using gas with different sticking factor, an accurate characterization of chambers of different geometries is always possible. Moreover the evaluation of the

transmission was performed using the ratio between both total and partial pressures, putting in evidence that, for gas with high sticking factor such as CO, total pressure transmission gives not exploitable results, thus making the use of partial pressure transmission and the installation of an RGA at the end of the chamber absolutely necessary.

Finally a cross analysis of the data collected in the LHC and in Building 113 explained the pressure decreasing trend in the machine. It was observed and calculated that the outgassing of the module housing the BA gauge decreases faster than the pumping speed of the NEG coated chambers, resulting in a diminution of the ultimate pressure values after every venting, bake-out and activation cycle. It implies that the future interventions will bring to an improvement of the vacuum performances in the LHC. Furthermore the NEG Pilot Sector, a system installed in the LSS of the LHC, was presented and described. Its purpose is to measure the saturation of the NEG coating due to the dynamic effects of the beam. The saturation is determined injecting H_2 by mean of a NEG cartridge and measuring the resulting transmission values. The results obtained with the NEG Pilot Sectors will allow to plan the interventions of NEG re-activation in the future Long Shutdowns.

Bibliography

[1] http://www.cern.ch/.

[2] R. Voss A. Breskin. *The CERN Large Hadron Collider: Accelerator and Experiments - Vol 1: LHC Machine, ALICE and ATLAS*. CERN, 2009.

[3] C. Benvenuti. Non-evaporable getters: from pumping strips to thin film coatings. In *EPAC*, volume 98, pages 200–204, 1998.

[4] G. Brumfiel. Eight-month delay for lhc. *Nature*, October 2014.

[5] F. Cicoira Y. L'Aminot C. Benvenuti, P. Chiggiato. Nonevaporable getter films for ultrahigh vacuum applications. *Journal of Vacuum Science & Technology A*, 16(1):148–154, 1998.

[6] P. Costa Pinto A. Escudeiro Santana T. Hedley A. Mongelluzzo V. Ruzinov I. Wevers C. Benvenuti, P. Chiggiato. Vacuum properties of tizrv non-evaporable getter films. *Vacuum*, 60(1):57–65, 2001.

[7] R.S. Calder. Ion induced gas desorption problems in the isr. *Vacuum*, 24(10):437–443, 1974.

[8] P. Chiggiato F. Cicoira A. Escudeiro Santana V. Johanek V. Ruzinov J. Fraxedas C.Benvenuti, J.M. Cazeneuve. A novel route to extreme vacua: the non-evaporable getter thin film coatings. *Vacuum*, 53(1):219–225, 1999.

[9] P. Chiggiato. Dégazage des solides en ultravide: quelques notions de base pour les techniciens du cern. Technical report, 2012.

[10] P Chiggiato and P Costa Pinto. Ti–zr–v non-evaporable getter films: From development to large scale production for the large hadron collider. *Thin Solid Films*, 515(2):382–388, 2006.

[11] A. Morris D.J. Hucknall. *Vacuum technology: calculations in chemistry*. Royal society of chemistry, 2003.

[12] R. Saban S. Baird A.L. Perrot K. Foraz F. Bordry, J.Ph. Tock. The first long shutdown (ls1) for the lhc. In *Conf. Proc.*, volume 130512, page MOZB202, 2013.

[13] R. Gevaud G. Baret. Helium leak detector, August 30 1994. US Patent 5,341,671.

[14] P. Chiggiato G. Bregliozzi, V. Baglin. Assessment of new components to be integrated in the lhc room temperature vacuum system. Technical report, 2014.

[15] V. Baglin J.M. Jiménez S. Blanchard K. Weiss G. Bregliozzi, J. Hansen. Achievement and evaluation of the beam vacuum performance of the lhc long straight sections. Technical report, 2008.

[16] R. Kersevan and J.L. Pons. Introduction to molflow+: New graphical processing unit-based monte carlo code for simulating molecular flows and for calculating angular coefficients in the compute unified device architecture environment. *Journal of Vacuum Science & Technology A*, 27(4):1017–1023, 2009.

[17] Chien-Cheng Li, Jow-Lay Huang, Ran-Jin Lin, and Ding-Fwu Lii. Preparation and characterization of non-evaporable porous ti–zr–v getter films. *Surface and Coatings Technology*, 201(7):3977–3981, 2006.

[18] R. Kersevan M. Ady. Introduction to the latest version of the test-particle monte carlo code molflow+. Technical report, 2014.

[19] F. Mazzolini. The use of neg pumps and coatings in large vacuum systems: experience and limitations. 2007.

[20] F. Caspers J.M Jimenez H. Day M. Garlaschè N. Magnin M. Taborelli L. Ducimetière J. Uythoven et. al. M.J. Barnes, P. Adraktas. Upgrade of the lhc injection kicker magnets. Technical report, 2013.

[21] T. Porcelli. Methods for saturation assessment in the lhc neg-coated beam pipes. 2012.

[22] A. Prodromides. *Non-evaporable getter thin film coatings for vacuum applications*. PhD thesis, EPFL–Lausanne, 2002.

[23] A. Rossi. Vasco (vacuum stability code): multi-gas code to calculate gas density profile in a uhv system. Technical report, 2004.

[24] C. Benvenuti S. Calatroni J. Carver P. Chiggiato H. Neupert W. Vollenberg S. Amorosi, M. Anderle. Study of the discharge gas trapping during thin-film growth. *Vacuum*, 60(1):89–94, 2001.

[25] K. Couturier N. Hilleret JR. Knaster P. L'Epeule M. Taborelli R. Veness L. Vos S. Calatroni, F. Caspers. Design aspects of the rf contacts for the lhc beam vacuum interconnects. In *Particle Accelerator Conference, 2001. PAC 2001. Proceedings of the 2001*, volume 3, pages 2168–2170. IEEE, 2001.

[26] J.M. Lafferty S. Dushman. *Scientific foundations of vacuum technology*. 1962.

[27] B. Salvant. Heat load from impedance on existing and new hw in the lhc era (including effect of flat bunches). Technical report, 2013.

[28] L. Schulz. Sputter-ion pumps. Technical report, Cern, 1999.

[29] G. Bregliozzi G. Lanza P. Chiggiato V. Baglin, JM. Jimenez. Cern vacuum-system activities during the long shutdown 1: The lhc beam vacuum. Technical report, 2014.

List of Figures

List of Tables